



Original Paper

# Characterization and Quantification of Mining-Induced Fractures in Overlying Strata: Implications for Coalbed Methane Drainage

Bichuan Zhang,<sup>1,2</sup> Haitao Sun,<sup>3,4,5</sup> Yunpei Liang,<sup>1,2,5</sup> Kequan Wang,<sup>3,4</sup> and Quanle Zou<sup>1,2</sup>

Received 9 August 2019; accepted 20 November 2019  
Published online: 7 December 2019

Coalbed methane (CBM) production in the overlying strata of coal reservoirs is often hampered by the unknown distribution of the mining-induced fractures. Mining-induced fractures are CBM migration pathways in the fractured overlying strata, and the excavation of coal seams within a mine causes the CBM in adjacent coal seams to flow into the overlying strata. The mining-induced fracture field in the overlying strata is the best place from which this CBM is drained. Here, to better understand the distributions of vertical and horizontal fractures caused by excavation, we propose a novel approach to quantify the dimensions of vertical and horizontal fractures in fractured zones. In addition, we demonstrate that there are negligible changes in the dimensions of horizontal fractures and great changes in the dimensions of vertical fractures when there is an increase in the height of the fractured zone. We further demonstrate that mining-induced angles mainly concentrate on 0°–10°, 50°–70°, 110°–120° and 170°–180°, and larger width fractures exist in both sides and top due to the de-stressed effect and fractures in the middle of model close under mining-induced stress. The approach described here could be used to improve the accuracy of cross-measure borehole positioning and the efficiency of CBM drainage.

**KEY WORDS:** Mining-induced fractures, Methane migration, Physical model test, Methane drainage, Voussoir beam structure.

## INTRODUCTION

Coalbed methane (CBM), shale gas and tight gas are considered important unconventional natural resources (Pan and Wood 2015; Li et al. 2018;

Peng et al. 2019a, b; Su et al. 2019; Yang et al. 2019; Zou et al. 2019, 2020). China is one of the leading coal-producing countries (Hein et al. 2019; Liu et al. 2019a, b). Unlike the geological histories and settings in North America and Australia, in China, coal reservoir permeability is often approximately 1 md (Palmer 2010). Draining CBM from low-permeability coal seams that store considerable resources is a challenging task, but mining-induced effects can improve the production of CBM resources. Long-wall mining is a widely used method in coal mining practice. This style of coal mining operation reduces the coal seam gas pressure and creates fractures in strata, enhancing CBM migration and capture from the working and surrounding coal seams (Guo et al.

<sup>1</sup>State Key Laboratory of Coal Mine Disaster Dynamics and Control, Chongqing University, Chongqing 400044, China.

<sup>2</sup>College of Resources and Safety, Chongqing University, Chongqing 400044, China.

<sup>3</sup>Gas Research Branch, China Coal Technology Engineering Group Chongqing Research Institute, Chongqing 400037, China.

<sup>4</sup>State Key Laboratory of the Gas Disaster Detecting Preventing and Emergency Controlling, Chongqing 400037, China.

<sup>5</sup>To whom correspondence should be addressed; e-mail: dreamsh@163.com, liangyunpei@126.com

2012; Wang and Ma 2019; Mostafa 2019). A caved zone, fractured zone and continuous deformation zone form in a vertical pattern during the excavation of a coal seam (Fig. 1). In the caved zone, the strata cave naturally due to loose rock blocks. In the fractured zone, the strata are divided by mining-induced fractures. In the continuous deformation zone, the strata deflect downward without the formation of obvious mining-induced fractures (Karaman et al. 2007; Miao et al. 2011). A considerable amount of scientific research has proven that mining-induced fractures are important in CBM production (Li et al. 2007; Ghabraie et al. 2015a, b; Ju et al. 2017, 2019). To improve the efficiency of CBM drainage, a better understanding of mining-induced fracture distribution is important.

Fractures have important effects in CBM drainage, coal seam extraction and other civil engineering (Liu et al. 2019a, b; Osterland and Weber 2019). Mining-induced fractures are CBM migration pathways. First, fractured areas were described as “O-shaped” zones in two-dimensional space (Qian and Xu 1998). After CBM flows into this de-stressed zone, achievement of sustained effective CBM drainage requires that cross-measure boreholes are drilled from the roadways to this region in the roof. This is the most widely accepted method in the Chinese mining industry. Later, mining-induced fractures were observed to form three-dimensional annular-shaped zones in the overburden and underburden (Guo et al. 2012; Feng et al. 2018). Mining-induced fractures in these zones can be described via the void ratio of fractures, based on evaluation of the subsidence of key strata (Wang et al. 2017a, b, c). However, it is difficult to determine the accurate position and dimensions of min-

ing-induced fractures and identify sweet spots for CBM drainage.

Physical and numerical modeling methods are the primary tools for investigating mining-related issues (Li et al. 2005). Numerical modeling techniques are more economical and quicker than physical modeling techniques, and numerical methods are more suitable for simulating detailed substrata behavior underground (Cinefra 2019; Tee and Kollahchi 2019). However, numerical models cannot solve all issues, and as problems become more complex, it will become increasingly difficult to represent true stratal responses with numerical methods (Zhu et al. 2011). This issue arises because of complexities of physical conditions. Physical modeling offers a powerful tool to yield important insights that cannot be gleaned from numerical models. Physical modeling illustrates the main principles that cause the phenomenon and solve complicated mining-related problems, such as surface subsidence (Thongprapha et al. 2015), substrata movement (Ghabraie et al. 2015a, b) and crack propagation (Wang et al. 2017a, b, c). The understanding of substrata movement mechanism provided by a physical model plays an important role in mining-induced fracture evolution and prediction in certain fields where numerical models are not available (Ghabraie et al. 2015a, b).

Fractured zones and three-dimensional annular-shaped zones are large pathways for methane drainage, and accurate positions of subsequent cross-measure boreholes cannot be easily determined. Accordingly, more attention should be paid to further quantification of mining-induced fractures to avoid inefficient methane drainage; hence, this study focused on mining-induced fractures in the fractured zone. Theoretical analysis was used to quantitatively describe the dimensions of horizontal and vertical fractures. In addition, physical model tests were conducted to investigate the characteristics of mining-induced fractures in terms of their fracture evolution. Some recommendations were made to improve the accuracy of cross-measure borehole positions to provide a reference for effective CBM drainage.

## THEORETICAL ANALYSIS OF MINING-INDUCED FRACTURE DISTRIBUTION

Mining-induced fractures are gradually formed with movement of substrata during longwall coal retreat mining. There are many kinds of substrata

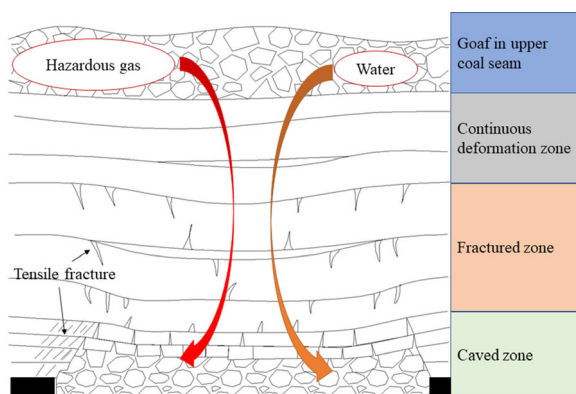


Figure 1. Failure characteristics of overlying strata in a longwall panel (Peng 2020).

movement styles, such as substrata deformation and bed separation (Ghabraie et al. 2015a, b). In terms of mechanics, mining-induced fractures are formed due to bending tensile and shear failure; bending tensile failure leads to the initiation of horizontal and vertical fractures, and shear failure promotes the development of such fractures (Alber et al. 2009).

**Model and Research Hypothesis**

In the direction of mining advance, overlying strata are divided into the coal pillar-supporting zone, separation zone and re-compacted zone, according to the mining-induced stress and fracture distributions (Qu et al. 2015). To quantify the mining-induced fractures in the fractured zone, it is necessary to make some assumptions. These assumptions are as follows:

- i. The dip angle of the model is 0°, and the blocks in the model are rigid.
- ii. The substrata model in the fractured zone fits the voussoir beam structure (Ju and Xu 2013).
- iii. The fractured rock shapes are identical and rectangular.
- iv. The touch point between blocks is at the middle of the downward block in the right-most block.
- v. The overlying strata model contains only horizontal and vertical fractures.

A simplified model of one side of mining-induced fractures in overlying strata can be obtained by the above assumptions (Fig. 2). In this model, horizontal fractures form in different substrata layers (Palchik 2005), and vertical fractures exist between the fractured rock blocks in the same substrata layer (Karacan et al. 2007). With the increase in the distance between the coal seam and substrata, the number of fractured rocks decreases (Wang et al. 2017a, b, c).

**Touch Point Coordinates in an Inclined Profile**

To calculate the coordinates of the touch points conveniently, it is necessary to choose the lower-left corner of the bottom-left block as the origin of the coordinate system. In the horizontal direction, the

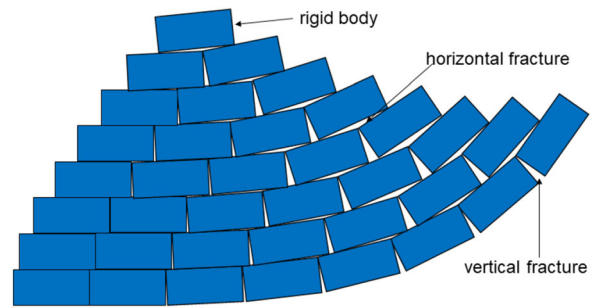


Figure 2. A simplified model of mining-induced fractures.

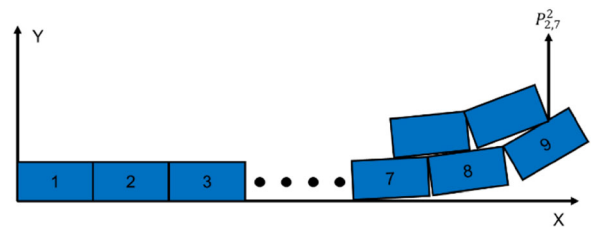


Figure 3. Establishment of a coordinate system.

positive direction is to the right, and in the vertical direction, the positive direction is upward. Figure 3 shows the whole coordinate system.

The touch point coordinates in the first layer of the substrata are obtained as:

$$\begin{cases} x_{1,i-1,i} = l \sum_{i=2} \cos \theta_{1,i} - f \sum_{i=2} \cos \theta_{1,i} \\ y_{1,i-1,i} = l \sum_{i=2} \sin \theta_{1,i} + f \sum_{i=2} \cos \theta_{1,i} \end{cases} \quad (1)$$

where subscripts  $i - 1$  and  $i$  stand for the  $(i - 1)$ th and  $i$ th blocks,  $x_{1,i-1,i}$  is the horizontal touch point coordinate between the  $(i - 1)$ th and  $i$ th blocks in the first substrata layer,  $y_{1,i-1,i}$  is the vertical touch point coordinate between the  $(i - 1)$ th and  $i$ th blocks in first substrata layer,  $l$  is the length of a rigid block,  $f$  is the width of a rigid block, and  $\theta_{1,i}$  is the angle of the block to the horizontal direction. To calculate the touch point coordinates above the first block layer, the coordinates in the rightmost block of the second layer of strata must be obtained as:

$$\begin{cases} x_{2,7}^2 = x_{1,7,8} - \frac{1}{2} \cos \theta_{1,8} \\ y_{2,7}^2 = y_{1,7,8} + \frac{1}{2} \cos \theta_{1,8} \end{cases} \quad (2)$$

where  $x_{2,7}^2$  is the horizontal coordinate of the rightmost block in the second layer of strata and  $y_{2,7}^2$  is

the vertical coordinate of the rightmost block in the second layer of strata. Then, the touch point coordinates in the second layer of strata are expressed as:

$$\begin{cases} x_{2,i-1,i} = x_{2,7,8} - l \sum_{i=2} \cos \theta_{2,i} \\ y_{2,i-1,i} = y_{2,7,8} - l \sum_{i=2} \cos \theta_{2,i} \end{cases} \quad (3)$$

Finally, the coordinates of all whole model touch points can be obtained as:

$$\begin{cases} x_{n,9-n}^2 = x_{n,9-n,10-n} - \frac{l}{2} \sum_{i=1} \cos \theta_{i,9-n} \\ y_{n,9-n}^2 = y_{n,9-n,10-n} + \frac{l}{2} \sum_{i=1} \cos \theta_{i,9-n} \\ x_{n,9-n,10-n} = x_{n,9-n}^2 - f \sin \theta_{n,8-n} \\ y_{n,9-n,10-n} = y_{n,9-n}^2 - f \sin \theta_{n,8-n} \\ x_{n,i-1,i} = x_{n,9-n,10-n} - l \sum_{i=2} \cos \theta_{n,i} \\ y_{n,i-1,i} = y_{n,9-n,10-n} - l \sum_{i=2} \cos \theta_{n,i} \end{cases} \quad (4)$$

where  $n$  represents the  $n^{th}$  layer of the substrata.

### Quantitative Analysis of Mining-Induced Fractures

According to the voussoir beam structure (Xu 2016), the change in  $\theta_{m,n}$  in the horizontal direction can be expressed as:

$$\theta_{m,i} = \theta_{m,1} \left(\frac{1}{4}\right)^{i-1} \quad (5)$$

where  $\theta_{m,n}$  is the angle of the  $i$ th rigid block to the horizontal direction in the  $m$ th layer of strata. The angle of the rightmost block to the horizontal direction in the second layer of strata is illustrated in Figure 4.

The angle of the rightmost rigid block in the  $(m - 1)^{th}$  layer of strata can be expressed as:

$$\theta_{2,7} = \arctan \frac{y_B - y_A}{x_B - x_A} \quad (6)$$

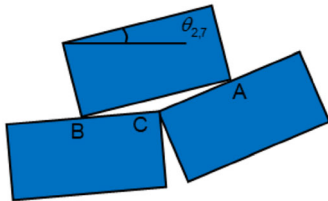


**Figure 4.** Angle of the rightmost block in the second layer relative to horizontal.

where  $x_A$  and  $x_B$  are the horizontal coordinates of points  $A$  and  $B$  and  $y_A$  and  $y_B$  are the vertical coordinates of points  $A$  and  $B$ . The angle between rigid blocks in the same layer of strata can be obtained as:

$$\begin{aligned} \alpha_{m,i-1,i} &= \theta_{m,i} - \theta_{m,i-1} = \theta_{m,i} - \frac{1}{4} \theta_{m,i} \\ &= \frac{3}{4} \theta_{m,i} = \frac{3}{4} \left(\frac{1}{4}\right)^{8-n-i} \theta_{m,9-n} \end{aligned} \quad (7)$$

where  $\alpha_{1,i-1,i}$  is the angle between the  $i$ th and  $(i - 1)$ th rigid blocks in the  $m$ th layer of strata. The width of the vertical fractures can be expressed as:

$$\begin{aligned} d_{m,i,i-1} &= 2f \sin \left(\frac{1}{2} \alpha_{m,i,i-1}\right) \\ &= 2f \sin \left[\frac{3}{8} \left(\frac{1}{4}\right)^{8-m-i} \theta_{m,9-m}\right] \end{aligned} \quad (8)$$

To determine the position of  $B$  in Figure 5, it is necessary to calculate the length of  $BC$  using the law of cosines. The length of  $BC$  can be expressed as:

$$a_{m,i,i-1} = \frac{1}{2} (-l \cos \alpha_{m,i,i-1} + \sqrt{l^2 \cos^2 \alpha_{m,i,i-1} + 3l^2}) \quad (9)$$

where  $a_{m,i,i-1}$  is the length of  $BC$  along the triangle. The  $b_{m,i,i-1}$  in the next triangle can be obtained as:

$$b_{m,i,i-1} = l - a_{m,i,i-1} - d_{m,i,i-1} \quad (10)$$

Inserting Eqs. 8 and 9 into Eq. 10 yields:

$$\begin{aligned} b_{m,i,i-1} &= l - \frac{1}{2} (-l \cos \alpha_{m,i,i-1} \\ &\quad + \sqrt{l^2 \cos^2 \alpha_{m,i,i-1} + 3l^2}) \\ &\quad - l \sin \left[\frac{3}{8} \left(\frac{1}{4}\right)^{8-m-i} \theta_{m,9-m}\right] \end{aligned} \quad (11)$$

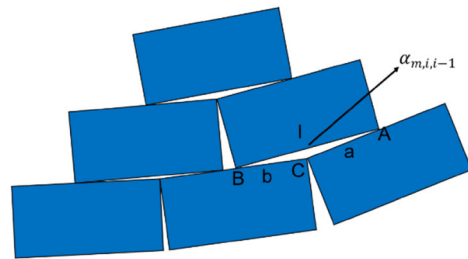


**Figure 5.** Theoretical calculation of the dimensions of a horizontal fracture.

The length of three sides of the triangle can be obtained as:

$$\begin{cases} b_{m,i,i-1} = l - a_{m,i,i-1} - d_{m,i,i-1} \\ \alpha_{m,i-1,i-2} = \frac{1}{4}\alpha_{m,i,i-1} \\ a_{m,i,i-1} = \frac{1}{2}(-l \cos \alpha_{m,i,i-1} + \sqrt{l^2 \cos^2 \alpha_{m,i,i-1} + 3l^2}) \end{cases} \quad (12)$$

The cross-sectional dimension of a horizontal fracture can be expressed as:

$$p_{m,i,i-1} = \frac{1}{2}(a_{m,i,i-1} + b_{m,i,i-1} + l) \quad (13)$$

$$S_{m,i,i-1} = \sqrt{p_{m,i,i-1}(p_{m,i,i-1} - a_{m,i,i-1})(p_{m,i,i-1} - b_{m,i,i-1})(p_{m,i,i-1} - l)} \quad (14)$$

where  $p_{m,i,i-1}$  is the half-length of the three sides and  $S_{m,i,i-1}$  is the dimension of a horizontal fracture.

Figure 6 shows the distribution of horizontal fractures in the inclined profile, as determined with MATLAB. The length of a rigid block is 10 m and the width of a rigid block is 5 m in this model, and the dimensions of the horizontal fractures are normalized by dividing by the maximum dimension of the horizontal fractures. The dimensions of horizontal fractures have negligible changes in the vertical direction, but considerable changes can be observed in the horizontal direction.

Suppose that the shape of the vertical fracture is an isosceles triangle; then, the dimension of the vertical fractures can be expressed as:

$$S'_{m,i,i-1} = \frac{1}{2}d_{m,i,i-1}f \cos\left(\frac{1}{2}\alpha_{m,i,i-1}\right) \quad (15)$$

By substituting Eqs. 7 and 8 into Eq. 15, the dimension of vertical fractures is written as:

$$S'_{m,i,i-1} = \frac{1}{2}f^2 \sin\left[\frac{3}{4}\left(\frac{1}{4}\right)^{8-m-i} \theta_{m,9-m}\right] \quad (16)$$

Figure 7 shows the distribution of vertical fractures in the inclined profile determined with MATLAB. The length of the rigid block is 10 m and the width of the rigid block is 5 m in the model, and the dimensions of the horizontal fractures are normalized by dividing by the maximum dimension of the vertical fractures. The dimensions of the vertical fractures change considerably in the vertical direction, and they also changes greatly in the horizontal direction.

### PHYSICAL MODELING OF MINING-INDUCED FRACTURES

Mining-induced fractures exist in overlying strata after retreating mining. It is challenging and expensive work to determine the characteristics of

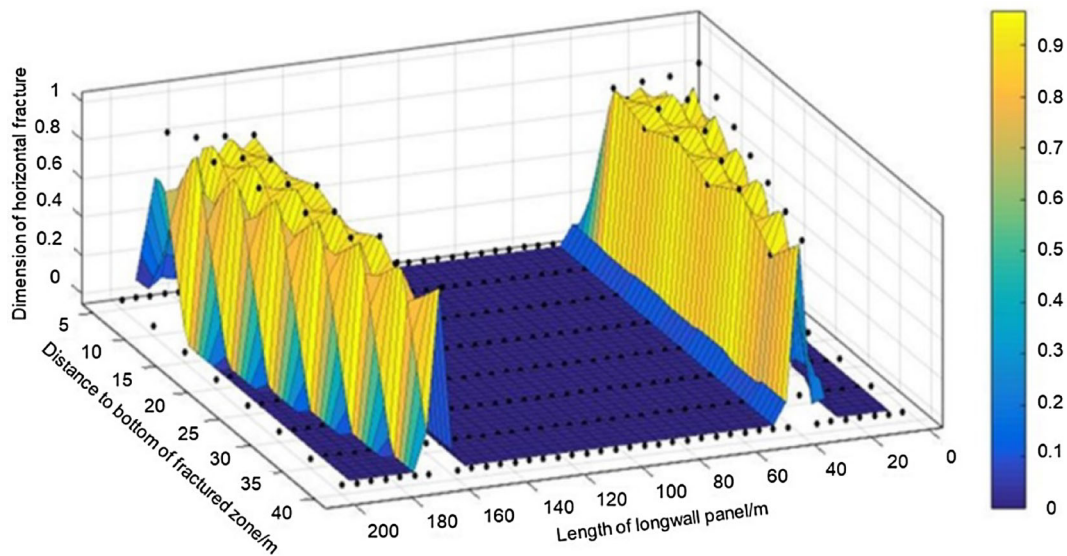


Figure 6. Normalized dimensions of horizontal fractures in an inclined profile.



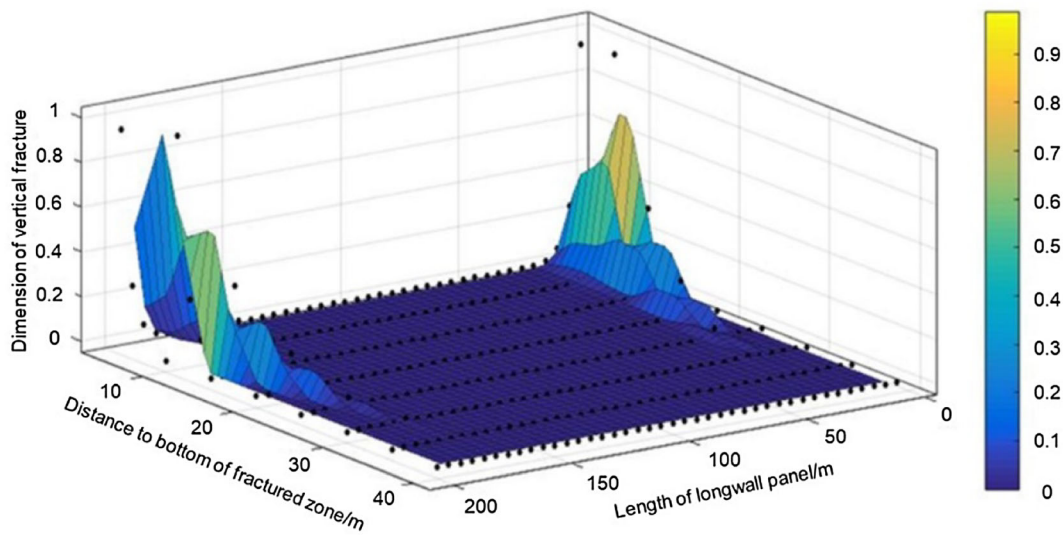


Figure 7. Normalized dimensions of vertical fractures in an inclined profile.

these fractures, and it is difficult to identify the overall distribution of mining-induced fractures. Physical modeling tests are advantageous in investigating the evolution of mining-induced fractures. The key of physical modeling tests is choosing a suitable similar material that can behave in a way similar to that of the real material being investigated (Ghabraie et al. 2015a, b). The similar material varies depending on the research problems. However, the density and strength of the similar material and the dimensions of the model should satisfy the similarity theory. Only under such conditions can a real case be simulated accurately and downscaled in time and space.

### Similarity Theory

A physical model must satisfy some similarity requirements, such as the strength and density of the material and geometry of the problem. This theory requires that some similarity coefficients must be constants, which are defined as the ratios of prototype parameters to model parameters (Zhu et al. 2011). These coefficients must satisfy the fundamental requirements of the similarity theory as (Fumagalli and Emanuele 2013):

$$\frac{C_\sigma}{C_\rho \times C_L} = 1 \quad (17)$$

$$C_L = L_p/L_m, \quad C_\sigma = \sigma_p/\sigma_m, \quad C_\rho = \rho_p/\rho_m \quad (18)$$

where  $C_L$ ,  $C_\sigma$  and  $C_\rho$  are the constants of the geometry, strength and density similarity, respectively, between the prototype and model,  $L$  is the length of the model,  $\sigma$  stands for compressive strength,  $\rho$  is density, and subscripts  $p$  and  $m$  stand for prototype and model, respectively. In this study,  $C_L$ ,  $C_\sigma$  and  $C_\rho$  are 100, 1.56 and 156, respectively.

### Mining and Methane Release Conditions

In this study, a physical model was constructed based on the geological condition of the 4308 longwall panel at the Cheng Zhuang Coal Mine, Northwest China. The depth of the overburden was between 350 and 400 m. The 4308 longwall panel was approximately 900 m long and 250 m wide. The #3 coal seam has an averaged thickness of 6 m and was mined by means of full-seam, one-pass mining. Figure 8 shows a generalized stratigraphic column of the roof strata and was compiled from data collected from boreholes drilled from the surface and underground. The immediate roof of the coal seam was an 11-m coarse siltstone overlain by a 29-m-thick medium-grained sandstone. The methane emission from longwall panel 4308 was 145.97 m<sup>3</sup>/min, and the methane content ranged from 5.2 to 9.4 m<sup>3</sup>/t. A lower adjacent seam releases a large amount of

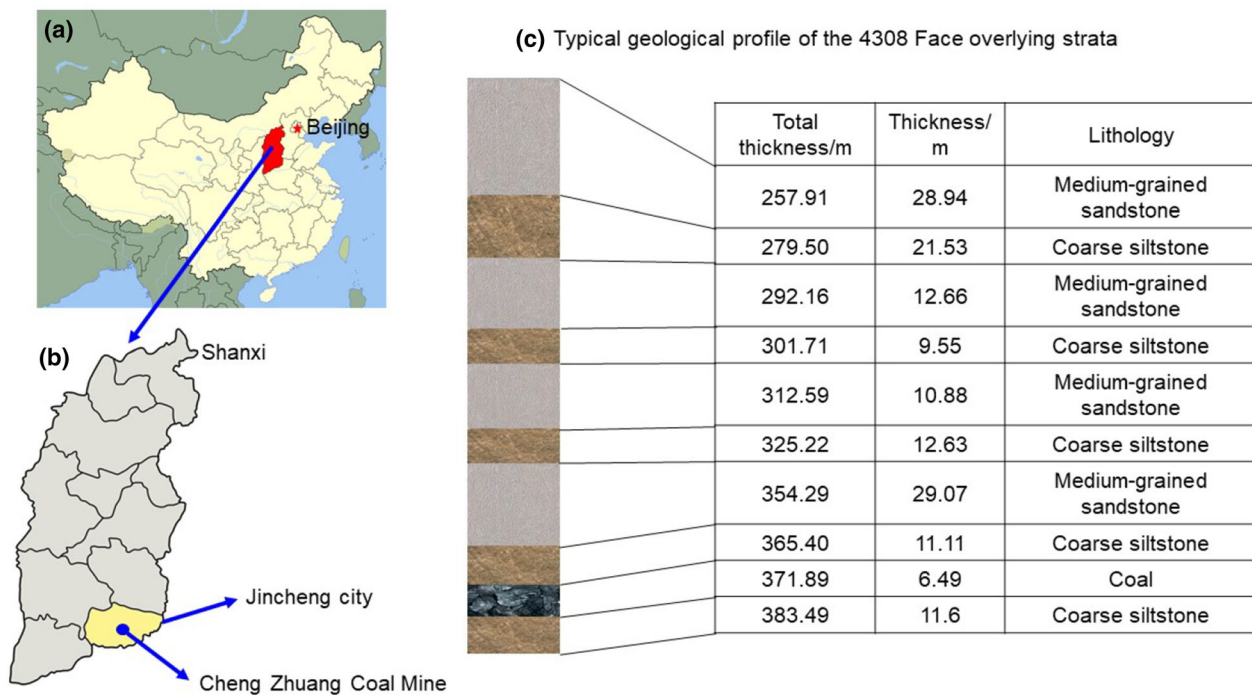


Figure 8. Location and typical geological profile of the 4308 longwall panel face overlying strata: (a) map of China; (b) map of Shanxi Province; (c) geological profile of overlying strata.

methane into the worked seam due to the effect of mining.

### Overlying Strata Collapse

The model has dimensions of 3.0 m × 0.4 m × 1.2 m in the *x*, *y* and *z* directions, respectively. This model was constructed layer by layer according to the required thickness of the similar material, which was calculated from the thickness of the real strata. The layers were separated by mica slices to simulate bedding planes. It took seven people and five days to construct the model. The experiment was conducted after the model completely finished three days later. Vertical stress corresponding to the in situ stress was applied via the top steel I-beam. The external loads were kept constant during the excavation stages.

Excavation started with a 250 mm cut in the coal seam. Longwall mining was performed stage by stage. In each stage, a 50-mm-long coal section was removed using a saw. The next excavation was performed an hour later, according to the constant of time similarity. This time corresponded to 4–6 h in

the real case. A total of 43 excavation stages were carried out continuously. The entire excavation took approximately 43 h.

The first roof collapse occurred at the second excavation stage, where the longwall panel had advanced 300 mm, corresponding to the 30-m-long coal seam extraction. Figure 9 shows the roof collapse pattern. Bed separation occurred during the second to third excavation stage. This was the first sign of substrata collapse, which occurred subsequently.

As the coal excavation continued, the immediate roof became a cantilever beam and collapsed when its length reached 750 mm (Fig. 10a). Vertical fractures formed in the substrata, and horizontal fractures, were observed between the intact strata and collapsed strata (Fig. 10a). Periodic substrata failure occurred during the excavation. These failures were limited to a certain height until the upper strata collapsed. A large horizontal fracture, which would store a large volume of high-concentration methane in reality, formed under the thick and hard strata (Fig. 10b). Such a region is known as a sweet spot in the methane drainage field.



**Characteristics of Mining-induced Fractures in a Fractured Zone**

In the three vertical zones mentioned above, the strata in the caved zone are unconsolidated and can be described as porous media with a methane flow field, and few mining-induced fractures exist in

the continuous deformation zone. However, the strata in the fractured zone can still be interconnected and may be a sweet spot for gas drainage. To investigate the flow characteristic in this region, the image of an advance of 150 cm was chosen as the research object (Fig. 11). This image was divided into 45 grid cells, whose length and width were 15 and 10 cm, respectively.

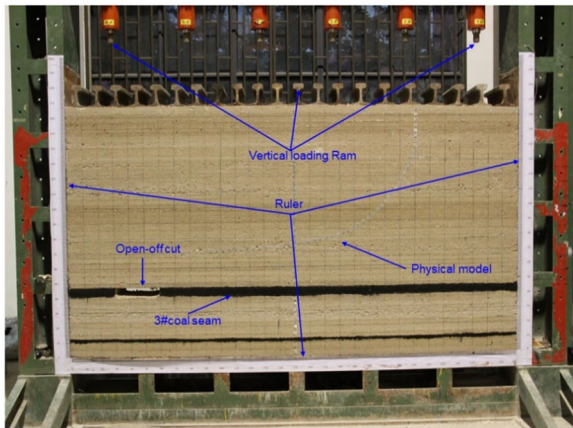


**Figure 9.** Physical modeling system for longwall mining.

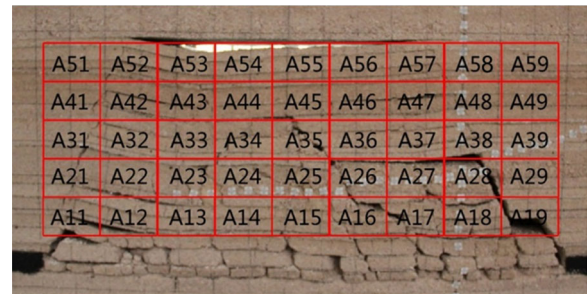


**Figure 11.** Grid diagram in the fractured zone.

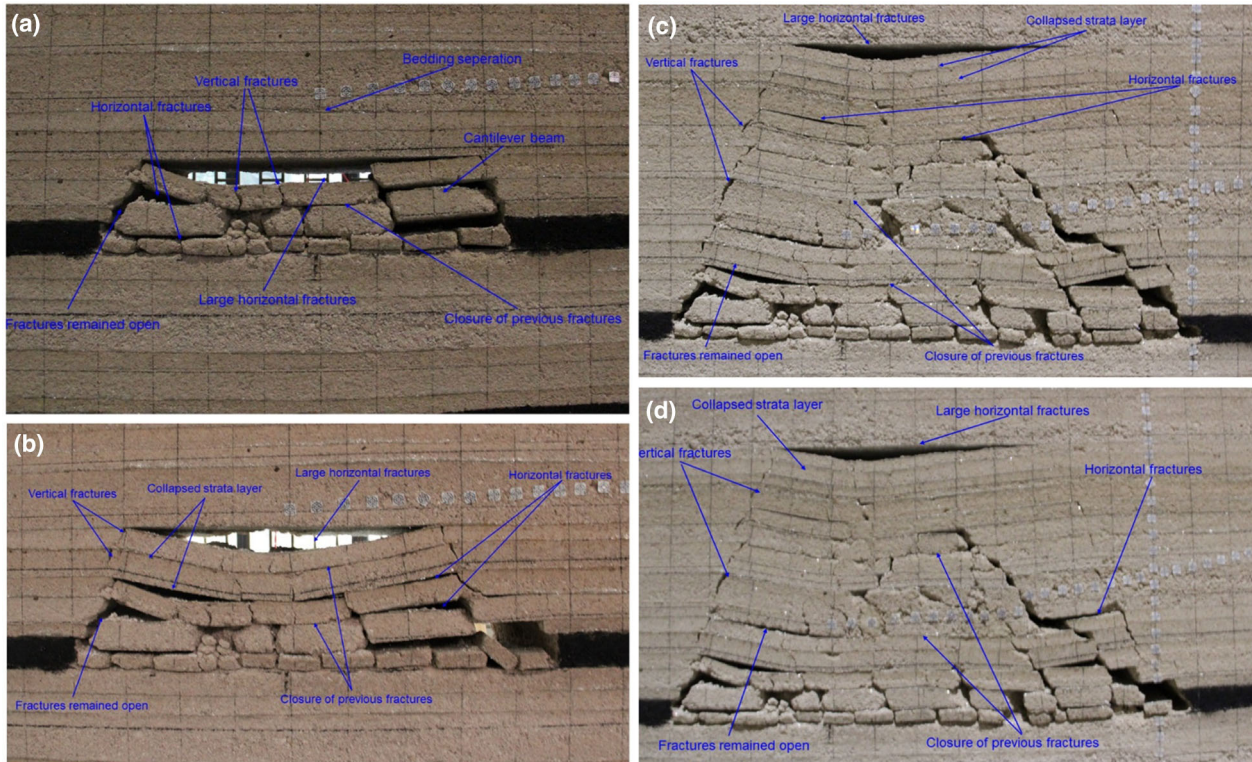


**Figure 10.** Physically simulated mining-induced fractures at different advance distances: (a) 75 cm, (b) 90 cm, (c) 120 cm, (d) 125 cm.



### Dimension of Mining-Induced Fractures

The result of the physical model was used to validate the theoretical model result of the estimation of the distribution of mining-induced fracture dimension. To obtain the mining-induced fracture dimension, first, the image of the physical model was transformed into a grayscale image (Fig. 12a); then, a binary image was obtained with MATLAB software (Fig. 12b). Finally, the dimensions of the mining-induced fractures were determined by counting the number of black points in every grid cell. The distribution of the mining-induced fracture is obtained via plotting the ratio of the number of black points to the total number of points in every grid of the model (Fig. 13).

### Distribution of Mining-Induced Fractures with Different Widths

The width of a fracture reflects its length, which dramatically affects fluid flow velocity. Figure 14 shows the distribution of mining-induced fracture widths through artificial statistics. There were 143 fractures in the model. Figure 14a and b shows fractures of smaller widths in every grid cell. However, fractures of larger widths exist on both sides and the top of the model in Figure 14c–g due to the de-stressed effect, and the fractures in the middle of model close under mining-induced stress. According to the cubic law (Witherspoon et al. 1980), flow velocity is sensitive to fracture width, and fractures of larger widths are mainly located on both sides of the lower fractured zone; hence, the lower fractured zone is the major region for methane flow.

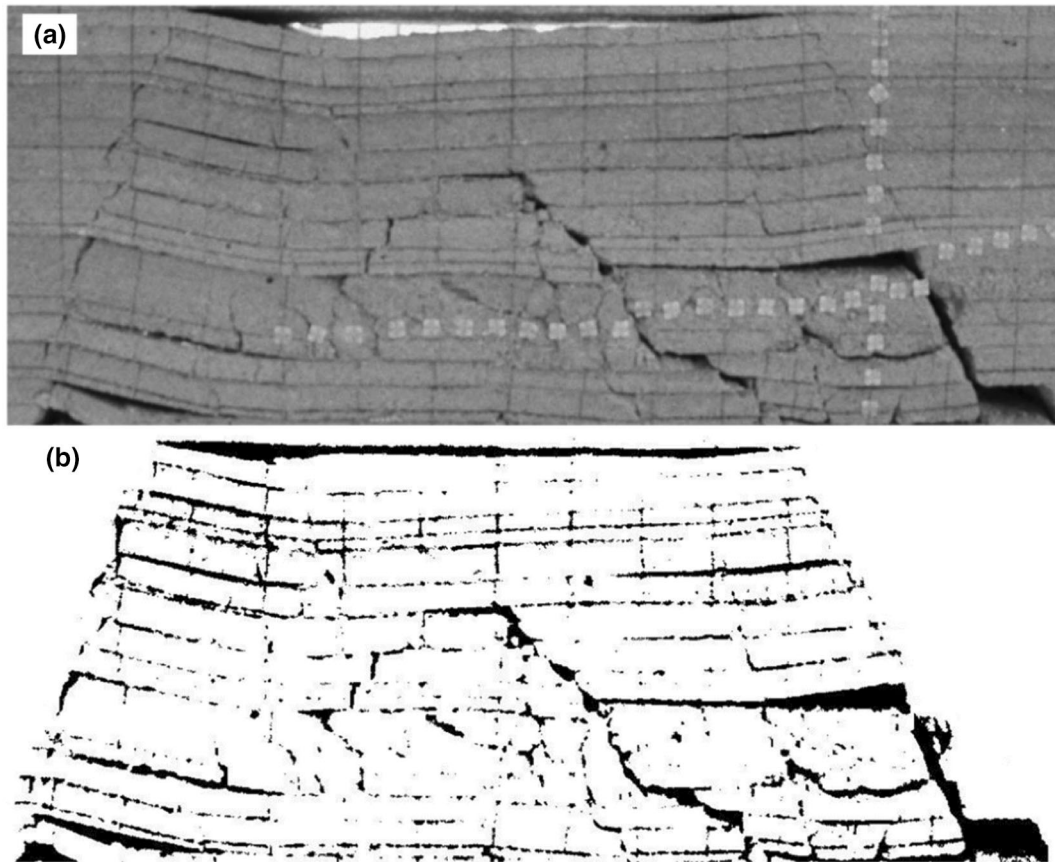


Figure 12. Images of mining-induced fractures: (a) grayscale and (b) binary.

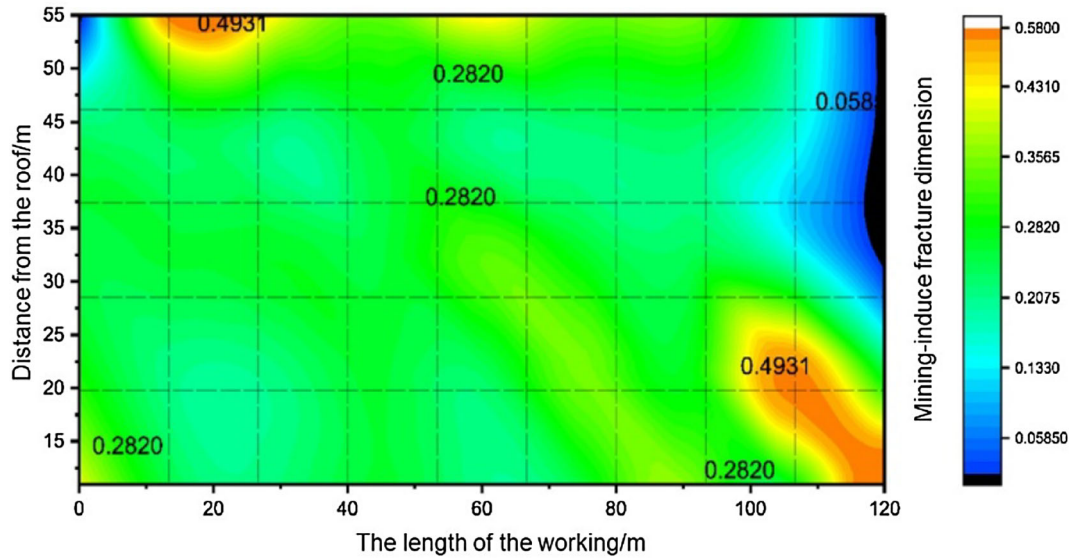


Figure 13. Distribution of mining-induced fracture dimension in the physical model.

### Distribution of the Angles of Mining-Induced Fractures

A rose diagram of joints directly displays many types of information, such as the number, angle and relationship of different fractures. The number of mining-induced fractures reflects the degree of influence of the mining practice (Wang et al. 2017a, b, c). With increasing distance from a coal seam, the degree of the mining effect decreases on both sides of the model (Fig. 15). The angle of mining-induced fractures is a fundamental parameter indicating the direction of fluid flow. Figure 15 shows the change in the angle and number of fractures in the vertical and horizontal directions. The angles of the fractures are mainly concentrated in the four intervals of  $0^{\circ}$ – $10^{\circ}$ ,  $50^{\circ}$ – $70^{\circ}$ ,  $110^{\circ}$ – $120^{\circ}$  and  $170^{\circ}$ – $180^{\circ}$ , which account for 82.3% of all the fractures, indicating that mining-induced fractures mainly consist of horizontal and vertical fractures. The ratio of the number of vertical and horizontal fractures to the total number of fractures is 43.5% in the lower fractured zone corresponding to grid cells A11, A12, A13, A21, A22 and A23; however, the ratio is 36.4% in the upper fractured zone corresponding to A31, A32, A33, A41, A42 and A43, indicating that the number of fractures in the vertical direction decreased on the sides of the fractured zone. The ratio in the middle of the fractured zone is much less than that at the

sides. These physical results suggest that the fluid flow direction is sub-horizontal and sub-vertical.

### GUIDING SIGNIFICANCE FOR COALBED METHANE DRAINAGE

The distribution of mining-induced fractures is a key factor that influences effective methane drainage. Therefore, quantification of mining-induced fractures, especially for high-methane and high-producing coal mines, is an important way to increase the efficiency of methane drainage. Our analysis indicates that the angle, density and width of mining-induced fractures concentrate on both sides of the model. Based on the geological conditions of the Cheng Zhuang coal mining area, some suggested techniques are as follows.

- i. Optimized selection of the cross-measure borehole bottom and overlying drainage zone positions: Mining-induced fractures exist at a relatively constant height on both sides of the strata overlying the coal seam. The highest dimension of mining-induced fractures is located at the inner boundary of the mining-influenced field of each layer of strata; this region may be a sweet spot.
- ii. Reasonable arrangement of cross-measure boreholes in the beginning of excavation:

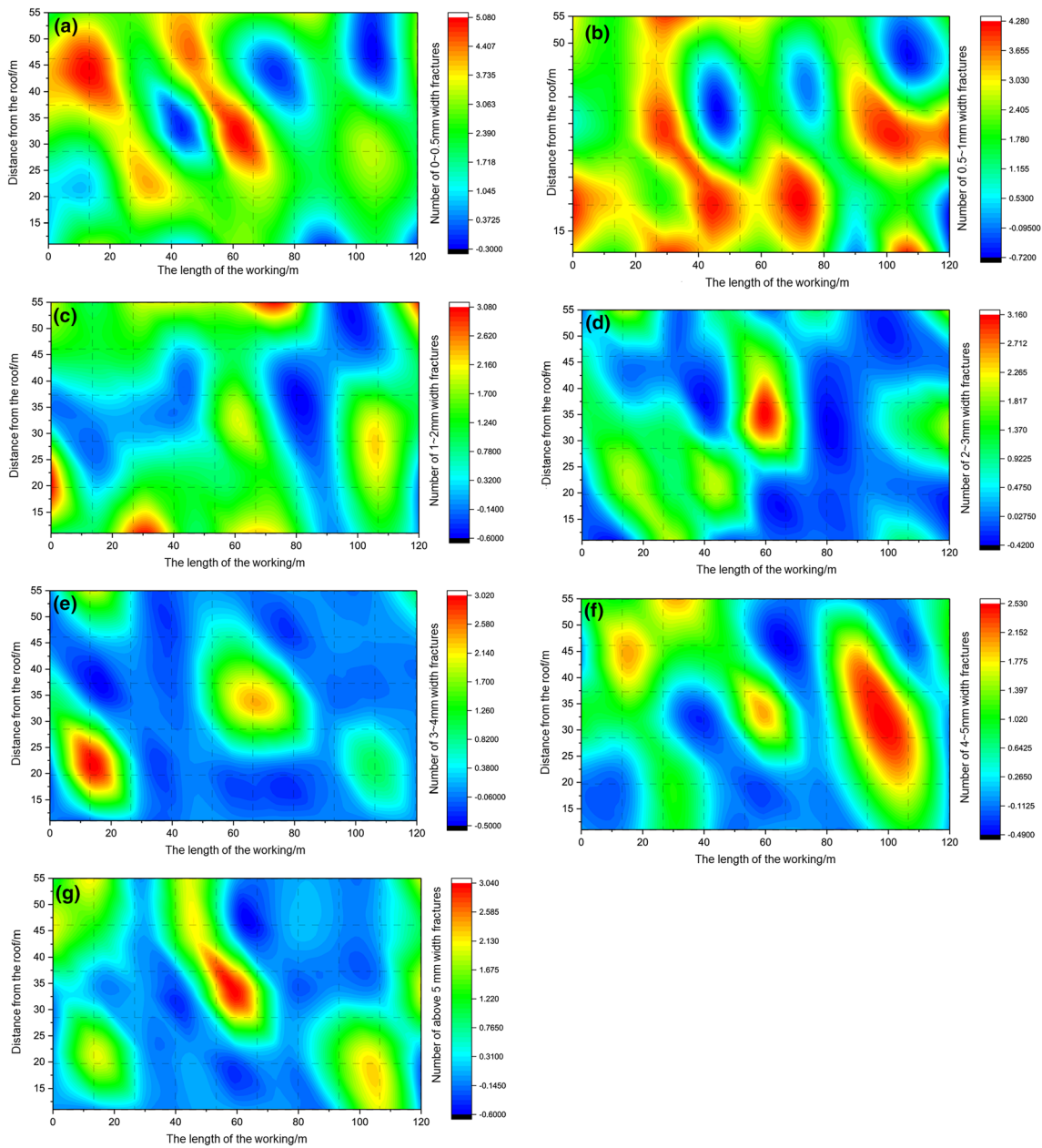


**Figure 14.** Distribution of fracture widths in inclined profiles: (a) 0–0.5 mm, (b) 0.5–1 mm, (c) 1–2 mm, (d) 2–3 mm, (e) 3–4 mm, (f) 4–5 mm, and (g) > 5 mm.

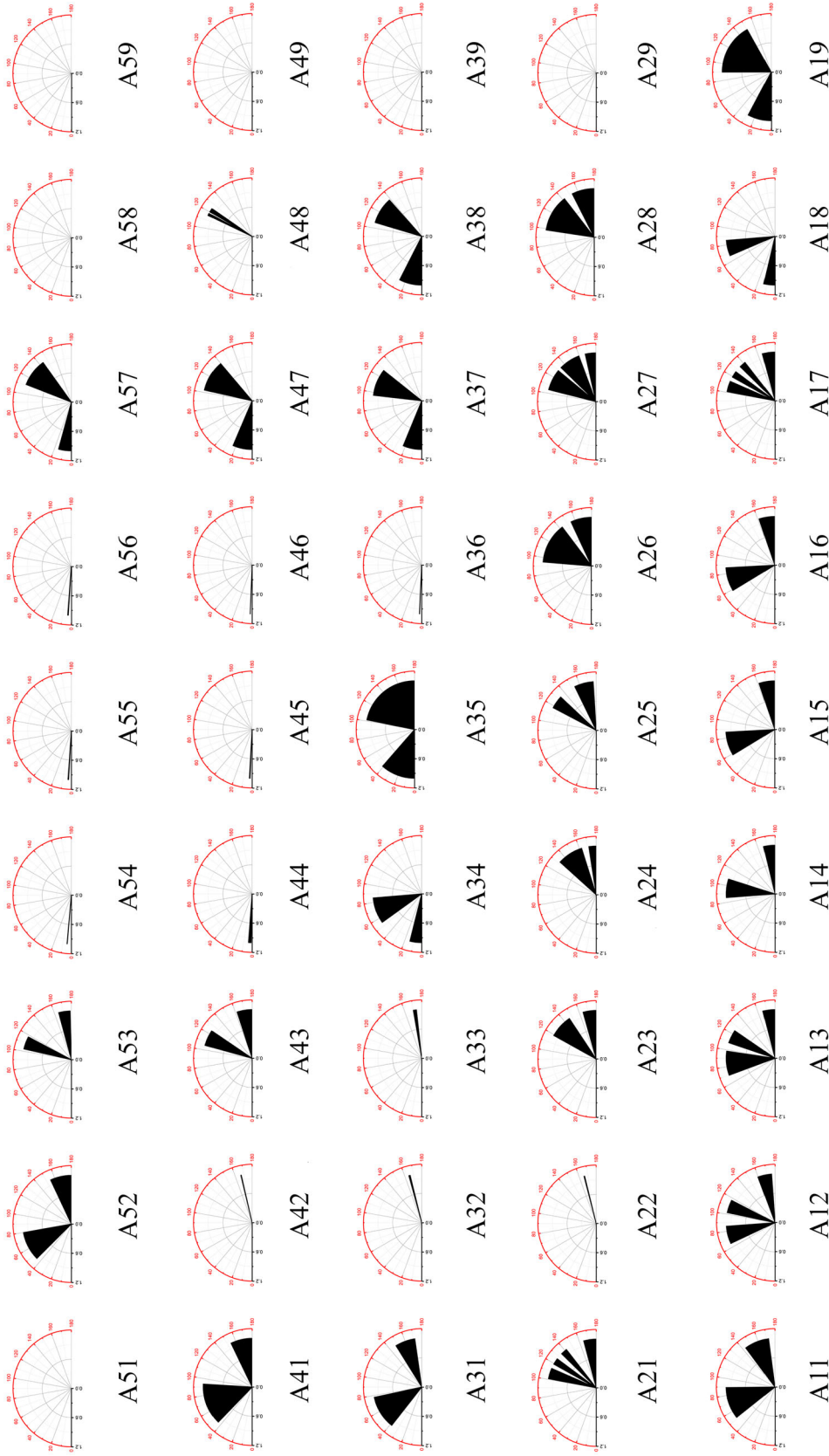


Figure 15. Rose diagrams of angles of joints in different grid cells.



Methane flow paths exist in the lower strata until full extraction is achieved. Therefore, arranging cross-measure boreholes or interpreting overlying drainage zones according to the evolution of mining-induced regions can increase drainage efficiency.

- iii. Full utilization of large mining-induced fractures under key strata: The movement of the strata depends on the key strata. Large fractures are produced due to the large difference in deformation between the key strata and the adjacent strata. Methane rises and diffuses into these fractures. Therefore, this deformation may create a sweet spot for draining of high concentrations of methane.

## CONCLUSIONS

The distribution of mining-induced fractures in the inclined profile of a fractured zone was investigated by means of a combination of physical modeling and theoretical analysis. The physical model was created based on a real case, and a theoretical model was created based on rigid body and voussoir beam structures. The results indicate that the theoretical model can capture the realistic distribution and dimensions of mining-induced fractures to some extent. Fractures with smaller widths are found throughout the region, and fractures with larger widths exist on both sides and at the top of the model. The physical and theoretical models suggest that large mining-induced fractures exist on both sides of the fractured zone. Considerable attention should be paid to the evolution of mining-induced fractures to determine the accurate positioning of boreholes for methane drainage. The angles and number of mining-induced fractures provide valuable information for the quantification of horizontal and vertical fractures.

## ACKNOWLEDGMENTS

This work is financially supported by the National Science and Technology Major Project of China (Grant No. 2016ZX05043005), the National Natural Science Foundation of China (51674050), and

Chongqing science and technology innovation leader talent support program (CSTCCXLJRC201911), which are gratefully acknowledged. The authors would like to thank Dr. Zou Quanle and their colleagues for their assistance during the physical modeling and data analysis.

## REFERENCES

- Alber, M., Fritschen, R., Bischoff, M., & Meier, T. (2009). Rock mechanical investigations of seismic events in a deep longwall coal mine. *International Journal of Rock Mechanics and Mining Sciences*, 46(2), 408–420.
- Cinefra, M. (2019). Numerical method for frequency response in visco-embedded nanoplate. *International Journal of Hydromechatronics*, 2(2), 119–130.
- Feng, L., Cao, S. G., Li, G. D., & Li, Y. (2018). Evolution of mine-induced stress concentration shell and stress relief body and its gas migration. *Journal of Mining & Safety Engineering*, 35(1), 155–162.
- Fumagalli, & Emanuele, (2013). *Statical and geomechanical models*. Berlin: Springer.
- Ghabraie, B., Ren, G., Smith, J., & Holden, L. (2015a). Application of 3D laser scanner, optical transducers and digital image processing techniques in physical modelling of mining-related strata movement. *International Journal of Rock Mechanics and Mining Sciences*, 80, 219–230.
- Ghabraie, B., Ren, G., Zhang, X. Y., & Smith, J. (2015b). Physical modelling of subsidence from sequential extraction of partially overlapping longwall panels and study of strata movement characteristics. *International Journal of Coal Geology*, 140, 71–83.
- Guo, H., Yuan, L., Shen, B. T., Qu, Q. D., & Xue, J. H. (2012). Mining-induced strata stress changes, fractures and gas flow dynamics in multi-seam longwall mining. *International Journal of Rock Mechanics and Mining Sciences*, 54, 129–139.
- Hein, F. J., Ambrose, W. A., Hackley, P., Mead, J. S., & American Association of Petroleum Geologists, E. (2019). Unconventional energy resources: 2017 review. *Natural Resources Research*, 28(4), 1661–1751.
- Ju, M., Li, X., Yao, Q., Liu, S., Liang, S., & Wang, X. (2017). Effect of sand grain size on simulated mining-induced overburden failure in physical model tests. *Engineering Geology*, 226, 93–106.
- Ju, Y., Wang, Y., Su, C., Zhang, D., & Ren, Z. (2019). Numerical analysis of the dynamic evolution of mining-induced stresses and fractures in multilayered rock strata using continuum-based discrete element methods. *International Journal of Rock Mechanics and Mining Sciences*, 113, 191–210.
- Ju, J. F., & Xu, J. L. (2013). Structural characteristics of key strata and strata behaviour of a fully mechanized longwall face with 7.0 m height chocks. *International Journal of Rock Mechanics and Mining Sciences*, 58, 46–54.
- Karacan, C. O., Esterhuizen, G. S., Schatzel, S. J., & Diamond, W. P. (2007). Reservoir simulation-based modeling for characterizing longwall methane emissions and gob gas venthole production. *International Journal of Coal Geology*, 71(2–3), 225–245.
- Li, T., Cai, M. F., & Cai, M. (2007). A review of mining-induced seismicity in China. *International Journal of Rock Mechanics and Mining Sciences*, 44(8), 1149–1171. <https://doi.org/10.1016/j.ijrmms.2007.06.002>.
- Li, X. L., Li, Z. H., Wang, E. Y., Liang, Y. P., Li, B., Chen, P., et al. (2018). Pattern recognition of mine microseismic and

- blasting events based on wave fractal features. *Fractals-Complex Geometry Patterns and Scaling in Nature and Society*, 26(3), 1850029.
- Li, Z. K., Liu, H., Dai, R., & Su, X. (2005). Application of numerical analysis principles and key technology for high fidelity simulation to 3-D physical model tests for underground caverns. *Tunnelling and Underground Space Technology*, 20(4), 390–399.
- Liu, C., Kubo, T., Lu, L., Koike, K., & Zhu, W. (2019a). Spatial simulation and characterization of three-dimensional fractures in Gejiu tin District, Southwest China. *Using GEO-FRAC. Natural Resources Research*, 28(1), 99–108.
- Liu, S. M., Li, X. L., Wang, D., & Zhang, L. (2019b). Mechanical and acoustic emission characteristics of coal at temperature impact. *Natural Resources Research*. <https://doi.org/10.1007/s11053-019-09562-w>.
- Miao, X. X., Cui, X. M., Wang, J. A., & Xu, J. L. (2011). The height of fractured water-conducting zone in undermined rock strata. *Engineering Geology*, 120(1–4), 32–39.
- Mostafa, S. (2019). Imputing missing values using cumulative linear regression. *CAAI Transactions on Intelligence Technology*, 4(3), 182–200.
- Osterland, S., & Weber, J. (2019). Analytical analysis of single-stage pressure relief valves. *International Journal of Hydromechatronics*, 2(2), 32–53.
- Palchik, V. (2005). Localization of mining-induced horizontal fractures along rock layer interfaces in overburden: Field measurements and prediction. *Environmental Geology*, 48(1), 68–80.
- Palmer, I. (2010). Coalbed methane completions: A world view. *International Journal of Coal Geology*, 82(3–4), 184–195.
- Pan, Z., & Wood, D. A. (2015). Coalbed methane (CBM) exploration, reservoir characterisation, production, and modelling: A collection of published research (2009–2015). *Journal of Natural Gas Science and Engineering*, 26, 1472–1484.
- Peng, S. S. (2020). *Longwall mining* (3rd ed.). London: CRC Press.
- Peng, K., Zhou, J. Q., Zou, Q. L., & Song, X. (2019a). Effect of loading frequency on the deformation behaviours of sandstones subjected to cyclic loads and its underlying mechanism. *International Journal of Fatigue*. <https://doi.org/10.1016/j.ijfatigue.2019.105349>.
- Peng, K., Zhou, J. Q., Zou, Q. L., Zhang, J., & Wu, F. (2019b). Effects of stress lower limit during cyclic loading and unloading on deformation characteristics of sandstones. *Construction and Building Materials*, 217, 202–2015.
- Qian, M., & Xu, J. (1998). Study on the “o shape” circle distribution characteristics of mining induced fractures in the overlying strata. *Journal of China Coal Society*, 23(5), 466–469.
- Qu, Q., Xu, J., Wu, R., Qin, W., & Hu, G. (2015). Three-zone characterisation of coupled strata and gas behaviour in multi-seam mining. *International Journal of Rock Mechanics and Mining Sciences*, 78, 91–98.
- Su, E., Liang, Y., Zou, Q., Niu, F., & Li, L. (2019). Analysis of effects of CO<sub>2</sub> injection on coalbed permeability: Implications for coal seam CO<sub>2</sub> sequestration. *Energy & Fuels*, 33(7), 6606–6615.
- Tee, K., & Kolahchi, R. (2019). Buckling analysis of piezoelectric cut out nanoplates using numerical method. *International Journal of Hydromechatronics*, 2(2), 99–111.
- Thongprapha, T., Fuenkajorn, K., & Daemen, J. J. K. (2015). Study of surface subsidence above an underground opening using a trap door apparatus. *Tunnelling and Underground Space Technology*, 46, 94–103.
- Wang, S., Li, X., & Wang, S. (2017a). Separation and fracturing in overlying strata disturbed by longwall mining in a mineral deposit seam. *Engineering Geology*, 226, 257–266.
- Wang, X., & Ma, L. W. (2019). Study on covering rough sets with topological methods. *CAAI Transactions on Intelligence Technology*, 4(3), 129–134.
- Wang, G., Wu, M., Wang, R., Xu, H., & Song, X. (2017b). Height of the mining-induced fractured zone above a coal face. *Engineering Geology*, 216, 140–145.
- Wang, H., Zhang, D., Wang, X., & Zhang, W. (2017c). Visual exploration of the spatiotemporal evolution law of overburden failure and mining-induced fractures: A case study of the Wangjialing coal mine in China. *Minerals*, 7(3), 35.
- Witherspoon, P. A., Wang, J. S. Y., Iwai, K., & Gale, J. E. (1980). Validity of cubic law for fluid-flow in a deformable rock fracture. *Water Resources Research*, 16(6), 1016–1024.
- Xu, J. L. (2016). *Distribution law of mining-induced strata fractures and applications*. Xu Zhou: China University of Mining and Technology Press.
- Yang, X., Wen, G., Dai, L., Sun, H., & Li, X. (2019). Ground subsidence and surface cracks evolution from shallow-buried close-distance multi-seam mining: A case study in Bulianta coal mine. *Rock Mechanics and Rock Engineering*, 52(8), 2835–2852.
- Zhu, W. S., Li, Y., Wang, S. G., & Zhang, Q. B. (2011). Quasi-three-dimensional physical model tests on a cavern complex under high in situ stresses. *International Journal of Rock Mechanics and Mining Sciences*, 48(2), 199–209.
- Zou, Q. L., Liu, H., Cheng, Z. H., Zhang, T. C., & Lin, B. Q. (2019). Effect of slot inclination angle and borehole-slot ratio on mechanical property of pre-cracked coal: Implications for ECBM recovery using hydraulic slotting. *Natural Resources Research*. <https://doi.org/10.1007/s11053-019-09544-y>.
- Zou, Q. L., Liu, H., Zhang, Y., Li, Q., Fu, J., & Hu, Q. (2020). Rationality evaluation of production deployment of outburst-prone coal mines: A case study of Nantong coal mine in Chongqing. *Safety Science*, 122.